Journal of Alloys and Compounds 509 (2011) 9230–9239

Contents lists available at ScienceDirect

Journal of Alloys and Compounds

journal homepage: www.elsevier.com/locate/jallcom

Spectroscopy features of Pr^{3+} and Er^{3+} ions in Li_2O–ZrO_2–SiO_2 glass matrices mixed with some sesquioxides

Ch. Srinivasa Rao [a], I.V. Kityk [b,*], T. Srikumar [a], G. Naga Raju [a], V. Ravi Kumar [a], Y. Gandhi [a], N. Veeraiah [a]

[a] Department of Physics, Acharya Nagarjuna University - Nuzvid Campus, Nuzvid-521201, A.P., India
[b] Electrical Engineering Department, Technical University of Czestochowa, Aleja Armii, Krajowej 17/19, PL-42-201 Czestochowa, Poland

ARTICLE INFO

Article history:
Received 19 June 2011
Received in revised form 30 June 2011
Accepted 1 July 2011
Available online 12 July 2011

Keywords:
Sesquioxides
Li_2O–ZrO_2–SiO_2 glass systems
Pr^{3+} and Er^{3+} ions
Spectroscopic features

ABSTRACT

The glasses of the composition Li_2O–ZrO_2–SiO_2: Pr_2O_3/Er_2O_3 mixed with three interesting sesquioxides (viz., Al_2O_3, Sc_2O_3, Y_2O_3) were synthesized. Optical absorption and fluorescence spectra (in the spectral range 350–2100 nm were studied at ambient temperature. The Judd–Ofelt theory was applied to characterize the absorption and luminescence spectra of Pr^{3+} and Er^{3+} ions in these glasses. Following the luminescence spectra, various radiative properties like transition probability A, branching ratio β and the radiative life time τ for different emission levels of two rare earth ions have been evaluated. The radiative life times for the upper levels $^3P_0$ (Pr^{3+}) and $^4S_{3/2}$ (Er^{3+}) have also been measured and quantum efficiencies were estimated. The variations observed in these parameters were discussed in the light of changing environment of rare earth ions due to mixing of different sesquioxides in the glass network.

1. Introduction

Among various rare earth ions, Pr^{3+} and Er^{3+} are attractive optical activators [1–3], which offer the possibility of simultaneous blue, green and red emission for laser action as well as IR emission for optical amplification. In fact, Pr-mixed glass fibers are being used as the most promising candidates for a 1.3 μm ($^1G_4 \rightarrow {}^3H_4$) communication window [1–3]. Up-conversion for example, yellow to blue, mechanism has also been demonstrated in some Pr^{3+} doped glasses under infrared laser pump [4–6]. Further, luminescence study of Pr^{3+} ion is more interesting to investigate since Pr^{3+} ion gives intense emission lines originating from three different levels ($^3P_0$, $^1D_2$ and $^1G_4$) [7].

Similarly, Er^{3+} ions give rich emission in the ultraviolet, visible and near infrared regions. This ion is more popular due to its transitions viz., $^4S_{3/2} \rightarrow {}^4I_{15/2}$ (green emission) and also $^4I_{13/2} \rightarrow {}^4I_{15/2}$ (NIR emission at 1.6 μm) which is being extensively used as an eye safe source in atmosphere, wind shear, laser radar, medical and surgery [8–10].

Among different silicate glass systems lithium silicates seemed to have adequate thermo-physical, chemical and mechanical stability to host rare earth ions for giving luminescence output over a wide range of wavelength [11,12]. Further, the addition of ZrO_2 to lithium silicate glasses is expected to improve the transparency over a wide range of wavelength (300 nm to 8 μm) and to increase the electrical resistivity and chemical inertness. It is also established that the inclusion of ZrO_2 to silicate glass matrix causes a substantial hike in the refractive index, decreases the cut-off wavelength and reduces the photochromism of the glass [13–15]. Such changes in physical properties make these glasses to offer good environment for hosting the rare earth ions to give luminescence emission with high efficiency.

When Li_2O–ZrO_2–SiO_2 glasses are mixed with different sesquioxides we may expect the structural modifications and local field variations around Ln^{3+} ion embedded in the glass network; such changes may have strong bearing on various luminescence transitions of lanthanide ions. In the present investigation, we have attempted to characterize the optical absorption and the fluorescence spectra of two lanthanide ions, viz., Pr^{3+} and Er^{3+} in lithium zirconium silicate glasses mixed with three interesting sesquioxides, viz., Y_2O_3, Sc_2O_3 and Al_2O_3. The presence of these oxides in lithium silicate glass network is observed to decrease the phonon energies and to pave the way for high luminescence efficiency [16,17]. Solid-state laser materials containing Y_2O_3 are proved to have the efficient operation both in continuous wave operation and in pulsed regimes. The mixing of Y_2O_3 to Li_2O–ZrO_2–SiO_2 glasses is expected to increase mechanical, thermal, and chemical stability and constitutes as a good candidate for biomedical and photonic applications [18,19]. In fact the addition of Y_2O_3 to silicate glass systems causes to widen the region of transparency, increases refractive index and opti-

* Corresponding author.
E-mail addresses: iwank74@gmail.com, ikityk@el.pcz.czest.pl (I.V. Kityk).

0925-8388/$ – see front matter © 2011 Elsevier B.V. All rights reserved.
doi:10.1016/j.jallcom.2011.07.001

cal band gap and good lattice match with Si ($a_{Y_2O_3} = 1.060$ nm, $a_{SiO_2} = 1.086$ nm); in view of these reasons the presence of Y_2O_3 in silicate glasses makes them as excellent host material for rare earth ions doping and a potential host for integrated optics [20–22].

Rare earth doped scandia (Sc_2O_3) glasses have been found to be interesting materials for many technological applications in the field of optical devices, such as luminescent displays, optical amplifiers and solid state lasers [23]. Scandium oxide, in particular, has recently attracted the attention of many researchers for its interesting physical and chemical properties. Its high chemical stability, together with a high bulk refractive index value and a high ultraviolet cut-off [24], makes it interesting for numerous applications in the field of photonics and optoelectronics. Further, due to its high thermal conductivity, trivalent rare earth doped scandia mixed glasses are very suitable host material for high power solid-state lasers [25,26]. Similarly considerable literature is available on emission features of different rare earth ions in Al_2O_3 mixed laser hosts [27–31].

2. Experimental

The following series of compositions are chosen for the present study.
Pr series:

LAlZSPr: $30Li_2O–9Al_2O_3–5ZrO_2–55SiO_2$: $1Pr_2O_3$
LScZSPr: $30Li_2O–9Sc_2O_3–5ZrO_2–55SiO_2$: $1Pr_2O_3$
LYZSPr: $30Li_2O–9Y_2O_3–5ZrO_2–55SiO_2$: $1Pr_2O_3$

Er series:

LAlZSEr: $30Li_2O–9Al_2O_3–5ZrO_2–55SiO_2$: $1Er_2O_3$
LScZSEr: $30Li_2O–9Sc_2O_3–5\ ZrO_2–55SiO_2$: $1Er_2O_3$
LYZSEr: $30Li_2O–9Y_2O_3–5ZrO_2–55SiO_2$: $1Er_2O_3$

Appropriate amounts of Analytical grade reagents of Li_2CO_3, ZrO_2, SiO_2, Al_2O_3, Sc_2O_3, Y_2O_3, Pr_6O_{11} and Er_2O_3 powders (Metall, China) all in mol% were thoroughly mixed in an agate mortar and melted in a platinum crucible in the temperature range of 1400–1450 °C in an automatic temperature controlled furnace for about 1/2 h. The resultant bubble free melt was then poured in a brass mould and subsequently annealed at 400 °C. The samples prepared were ground and optical polished to the dimensions of 1 cm × 1 cm × 0.2 cm. The amorphous nature of samples was verified by recording XRD using Rigaku D/Max ULTIMA III X-ray diffractometer with CuK_α radiation. Scanning electron microscopy studies were also carried out on these samples to observe the amorphous nature using HITACHI S-3400N Scanning Electron Microscope. The density d of the bulk samples was determined (to an accuracy of ±0.0001) by the standard principle of Archimedes' using o-xylene (99.99% pure) as the buoyant liquid. The mass of the samples was measured to an accuracy of 0.1 mg using Ohaus digital balance, Model AR2140 to evaluate the densities.

The refractive index (n_d) of the samples was measured (at $\lambda = 589.3$ nm) using Abbe refractometer with monobromo naphthalene as the contact layer between the glass and the refractometer prism. The optical absorption spectra of the samples were recorded at room temperature in the spectral wavelength range covering 300–2200 nm to a spectral resolution of 0.1 nm using JASCO Model V-670 UV–vis–NIR spectrophotometer. The photoluminescence spectra of the samples were recorded at room temperature on a Photon Technology International (PTI) Spectrofluorometer. This instrument contains auto calibrated quadrascopic monochrometer for wavelength selection and quadracentric sample compartment. The light source is high intensity continuous xenon lamp with high sensitivity TE-cooled InGaAs detector with lock-in amplifier and chopper for noise suppression and an additional emission mono with a 600 groove grating blazed at 1.2 μm. The system provides unmatched NIR luminescence recording capability from 500 nm to 2.2 μm. The spectral resolution is 0.1 nm. The fluorescence decay curves were recorded by using Jobinyvon spectrofluorolog-3 with pulsed xenon lamp of 450 W with pulse duration: 0.2–10 ms.

3. Results

It was ensured that the samples prepared were free from visible in homogeneities such as inclusions, cracks or bubbles. Based upon the visual examination, the absence of peaks in the X-ray diffraction pattern, absence of crystalline phases in SEM pictures, we could come to the conclusion that the samples prepared were of reasonably free from crystallinity.

From the measured values of the density d and average molecular weight $\bar{M}$ of the samples, various other physical parameters such as rare earth ion concentration N_i, mean rare earth ion separation r_i and molar volume are computed and presented in Table 1.

The optical absorption spectra (Fig. 1(a) and (b)) of Pr^{3+} doped $Li_2O–M_2O_3–ZrO_2–SiO_2$ glasses recorded at room temperature have exhibited the following absorption bands:

$$^3H_4 \rightarrow {}^3P_2, {}^3P_1, {}^3P_0, {}^1D_2, {}^3F_4, {}^3F_3 \text{ and } {}^3F_2$$

Out of these, $^3H_4 \rightarrow {}^3F_4, {}^3F_3, {}^3F_2$ transitions are found to be in the infrared region, $^3H_4 \rightarrow {}^1D_2$ in the orange region where as $^3H_4 \rightarrow {}^3P_2$, $^3P_1$, $^3P_0$ are in the violet and blue regions.

Similarly the spectra of all the three Er^{3+} doped glasses have exhibited the following absorption bands (Fig. 2(a) and (b)):

$$^4I_{15/2} \rightarrow {}^4G_{9/2}, {}^4G_{11/2}, {}^2H_{9/2}, {}^4F_{3/2}, {}^4F_{5/2}, {}^4F_{7/2}, {}^2H_{11/2}, {}^4S_{3/2}, {}^4F_{9/2}, {}^4I_{9/2}, {}^4I_{11/2} \text{ and } {}^4I_{13/2}$$

The replacement of sesquioxides one with other in the glass matrix is found to alter the spectral positions of various absorption bands of both the rare earth ions slightly; however considerable differences in the absorption strength under given peak (of the two rare earth ions) have been observed for three sesquioxides mixed glasses.

The experimental oscillator strengths (OS) of the absorption transitions are estimated from the absorption spectra in terms of the area under an absorption peak.

According to the conventional Judd–Ofelt (JO) theory [32,33], the calculated OS of the electric dipole transition between two states can be expressed as follows:

$$f_{cal} = \frac{8\pi^2 mc\nu\chi}{3h(2J+1)} \sum_{\lambda=2,4,6} \Omega_\lambda \left\langle f^N[\gamma, S, L]J \left\| U^\lambda \right\| f^N[\gamma', S', L']J' \right\rangle^2, \quad (1)$$

where m is the electron mass, c the speed of light, h is the Planck's constant, $\chi = (n^2+2)^2/9n$ the local field correction, n is the refractive index, and the bra- and ket-vectors $\left\langle f^N[\gamma, S, L]\, J \right|; \left| f^N[\gamma', S', L']\, J' \right\rangle \rangle$ stand for the initial and final states, respectively, with all necessary sets of quantum numbers in square brackets. $\left\| U^\lambda \right\|$ are the reduced matrix elements of the unit tensor operators calculated between the states involved into a considered transition.

In the case of Pr^{3+} doped glasses due to a strong mixture between the $4f^2$ and 4f 5d states the second order intensity parameter Ω_2 [34–37] is likely that negative. To overcome this drawback, the modified JO theory [38,39] has been used:

$$f_{cal} = \frac{8\pi^2 mc\nu\chi}{3h(2J+1)} \sum_{\lambda=2,4,6} \times \left[1 + \frac{E_{J'} - 2E_f^0}{E_{5d} - E_f^0}\right] \Omega_\lambda \left\langle f^N[\gamma, S, L]J \left\| U^\lambda \right\| f^N[\gamma', S', L']J' \right\rangle^2, \quad (2)$$

where $E_{J'}$, E_{5d}, E_f^0 are the energies of the final state, lowest $4f^15d^1$ state, and the average energy of all $4f^2$ states of Pr^{3+}, respectively. All other entries have the same meaning as in Eq. (2). E_{5d} was taken as 48,385 cm^{-1} [40], and E_f^0 was set at 10,000 cm^{-1}. The summary of these parameters for the two rare earth doped glasses mixed with the three sesquioxides is presented in Tables 2a and 2b.

The $\left\| U^\lambda \right\|$ reduced matrix elements have been re-calculated, using literature data on the Pr^{3+} and Er^{3+} Hamiltonian parameters taken from Ref. [41]. The procedure of fitting of the calculated from Eq. (2) OS to those deduced from the experimental spectra is described in Ref. [42]. A set of matrix equations (which includes the

Table 1
Physical parameters of Li_2O–M_2O_3–ZrO_2–SiO_2: Ln_2O_3 glasses.

Glass→	Pr^{3+} doped glasses			Er^{3+} doped glasses		
Physical parameter↓	LAlZS	LScZS	LYZS	LAlZS	LScZS	LYZS
Density d (g/cm^3)	2.5243	2.5147	2.6151	2.5396	2.5300	2.6303
Dopant ion conc. N_i ($\times 10^{20}$ ions/cm^3)	2.51	2.37	2.19	2.50	2.37	2.19
Interionic distance R_i (Å)	15.86	16.16	16.58	15.87	16.17	16.59
Polaron radius R_p (Å)	6.39	6.51	6.68	6.40	6.51	6.68
Field strength F_i (10^{15}, cm^{-2})	0.735	0.708	0.672	0.733	0.707	0.672
Refractive index (n_d)	1.785	1.786	1.788	1.786	1.787	1.790
Molar volume V_m (cm^3 mol^{-1})	24.02	25.40	27.45	24.09	25.46	27.49

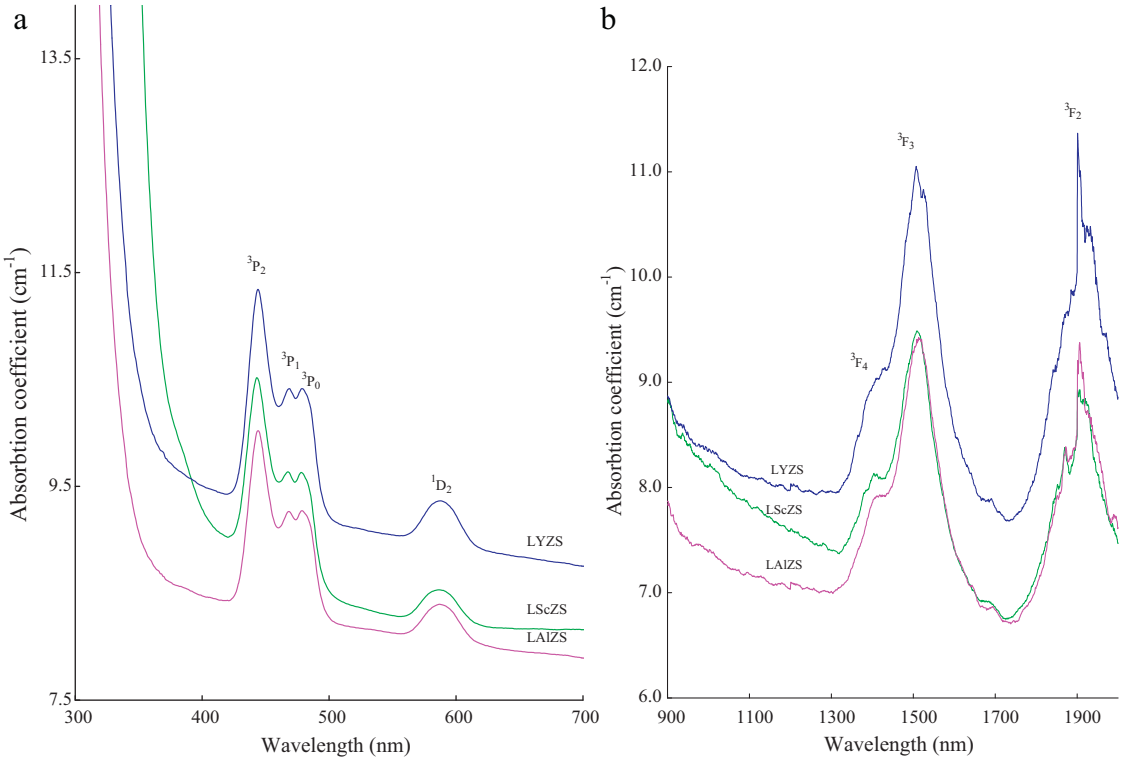

Fig. 1. (a) Optical absorption spectra of Pr^{3+} doped Li_2O–M_2O_3–ZrO_2–SiO_2 glasses recorded at room temperature in visible region. (b) Optical absorption spectra of Pr^{3+} doped Li_2O–M_2O_3–ZrO_2–SiO_2 glasses recorded at room temperature in NIR region.

U^2, U^4, and U^6 matrices, the matrices of the experimental OS and the energies of the corresponding transitions) should be solved to minimize the difference between the calculated f_{cal} and observed f_{exp} OS. The quality of fitting is determined by the root mean squared deviation (RMS) approach. The deviation indicates reasonably good fitting between theory and experiment demonstrating the applicability of JO theory. The summary of the JO parameters Ω_λ for Pr^{3+} and Er^{3+} doped Li_2O–M_2O_3–ZrO_2–SiO_2 glasses is presented in Table 3.

The values of Ω_λ are found to be in the following order for the Pr^{3+} doped glasses: $\Omega_6 > \Omega_4 > \Omega_2$ and for Er^{3+} the order is $\Omega_2 > \Omega_4 > \Omega_6$ for all the three sets of samples. The comparison of the data on Ω_λ parameters of Pr^{3+} and Er^{3+} ions in various other glass matrices [43–48] indicated the similar trends with few exceptions.

Table 2a
The absorption band energies, the oscillator strength for the transitions of Pr^{3+} ion Li_2O–M_2O_3–ZrO_2–SiO_2 glasses.

Transition	LAlZS glasses			LScZS glasses			LYZS glasses		
	Energy (cm^{-1})	f_{exp} ($\times 10^{-6}$)	f_{cal} ($\times 10^{-6}$)	Energy (cm^{-1})	f_{exp} ($\times 10^{-6}$)	f_{cal} ($\times 10^{-6}$)	Energy (cm^{-1})	f_{exp} ($\times 10^{-6}$)	f_{cal} ($\times 10^{-6}$)
$^3H_4 \rightarrow {}^3F_2$	5260	5.34	5.29	5247	5.62	5.34	5247	5.74	5.43
$\rightarrow {}^3F_3$	6640	22.14	22.67	6614	22.83	22.56	6636	22.34	22.37
$\rightarrow {}^3F_4$	7102	20.78	20.83	7123	20.82	20.88	7133	20.92	20.75
$\rightarrow {}^1D_2$	17,036	3.40	3.36	17,036	3.56	3.36	17,036	3.67	3.43
$\rightarrow {}^3P_0$	20,921	2.38	2.57	20,921	2.42	2.33	20,921	2.53	2.32
$\rightarrow {}^3P_1$	21,413	3.25	3.60	21,413	3.34	3.25	21,413	3.48	3.36
$\rightarrow {}^3P_2$	22,523	10.68	10.77	22,573	10.78	11.01	22,573	10.82	10.90
Rms deviation			±0.4675			±0.4771			±0.5613
Bonding parameter			−0.108			−0.115			−0.125

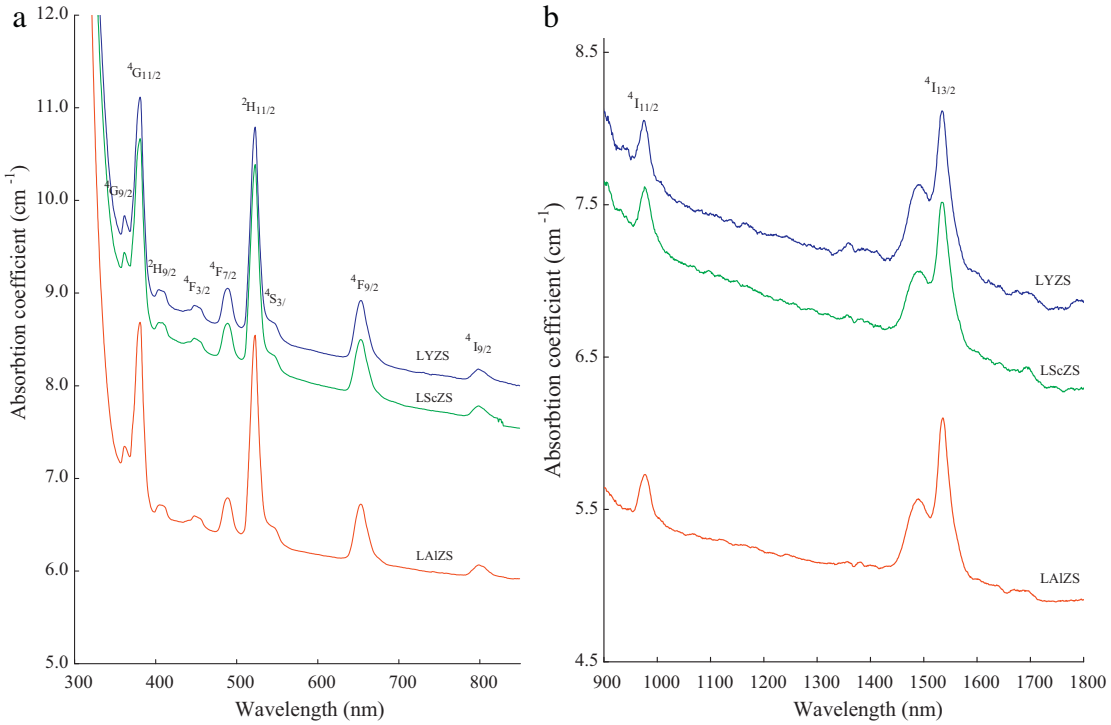

Fig. 2. (a) Optical absorption spectra of Er^{3+} doped Li_2O–M_2O_3–ZrO_2–SiO_2 glasses recorded at room temperature in the visible region. (b) Optical absorption spectra of Er^{3+} doped Li_2O–M_2O_3–ZrO_2–SiO_2 glasses recorded at room temperature in the NIR region.

Table 2b
The absorption band energies, the oscillator strength for the transitions of Er^{3+} ion in Li_2O–M_2O_3–ZrO_2–SiO_2 glasses.

Transition	LAlZS glasses			LScZS glasses			LYZS glasses		
	Energy (cm^{-1})	f_{exp} ($\times10^{-6}$)	f_{cal} ($\times10^{-6}$)	Energy (cm^{-1})	f_{exp} ($\times10^{-6}$)	f_{cal} ($\times10^{-6}$)	Energy (cm^{-1})	f_{exp} ($\times10^{-6}$)	f_{cal} ($\times10^{-6}$)
$^4I_{15/2} \rightarrow {}^4I_{13/2}$	6523	0.61	0.55	6523	0.76	0.72	6519	0.65	0.69
$\rightarrow {}^4I_{11/2}$	10,246	0.29	0.25	10,262	0.32	0.27	10,267	0.30	0.28
$\rightarrow {}^4I_{9/2}$	12,563	1.34	1.39	12,563	1.35	1.39	12,531	1.26	1.35
$\rightarrow {}^4F_{9/2}$	15,361	3.65	3.95	15,337	2.93	2.08	15,361	3.30	3.73
$\rightarrow {}^4S_{3/2}$	18,315	0.27	0.21	18,349	0.42	0.29	18,282	0.53	0.44
$\rightarrow {}^2H_{11/2}$	19,157	7.71	7.94	19,157	7.86	7.13	19,157	7.11	7.16
$\rightarrow {}^4F_{7/2}$	20,576	1.49	1.48	20,576	1.56	1.53	20,534	1.17	1.24
$\rightarrow {}^4F_{5/2}$	22,075	0.67	0.46	22,124	0.14	0.11	22,173	0.68	0.49
$\rightarrow {}^4F_{3/2}$	22,422	0.22	0.21	22,422	0.13	0.09	22,472	0.17	0.17
$\rightarrow {}^2H_{9/2}$	24,752	1.19	1.22	24,752	1.70	1.22	24,570	1.14	1.20
$\rightarrow {}^4G_{11/2}$	26,316	16.90	16.95	26,316	15.19	15.29	26,316	15.62	15.57
$\rightarrow {}^4G_{9/2}$	27,701	11.22	11.42	27,701	9.27	9.45	27,778	10.95	9.27
rms deviation			±0.1640			±0.4155			±0.5845
Bonding parameter (δ)			−0.2097			−0.2677			−0.2685

The bonding parameter (δ), defined as [49,50]

$$\delta = \left[\frac{1-\overline{\beta}}{\overline{\beta}}\right] \times 100, \quad (3)$$

is computed for all the glasses and presented in Tables 2a and 2b. In Eq. (3), $\overline{\beta} = \sum_{1N}\beta/N$ and β (the nephelauxetic ratio) = ν_c/ν_a. ν_c and ν_a are the energies in cm^{-1} of the corresponding transitions in the complex and aquo-ion respectively and N refers to the number of levels used to compute $\overline{\beta}$ values. The value of β is found to be more negative for Y_2O_3 mixed glasses when compared with that of other two glasses.

Table 3
The summary of J–O parameters Ω_λ ($\times10^{-20}$ cm^2).

Sesquioxides	Pr^{3+} doped glasses			Er^{3+} doped glasses		
	Ω_2	Ω_4	Ω_6	Ω_2	Ω_4	Ω_6
Al_2O_3	2.34	5.27	29.43	1.72	1.56	0.68
Sc_2O_3	2.21	4.27	27.12	1.68	1.53	0.65
Y_2O_3	2.08	4.21	26.34	1.60	1.40	0.52

The luminescence spectra of all the three glasses doped with Pr^{3+} and Er^{3+} ions recorded at room temperature in the visible and NIR regions are shown in Figs. 3(a) and (b) and 4(a) and (b) respectively; the spectra exhibited the following prominent emission bands:

Pr^{3+} (λ_{exc} = 442 nm) : $^3P_0 \rightarrow {}^3F_2$,
$^3H_6$, $^3H_4$, $^3H_5$; $^1D_2 \rightarrow {}^3H_4$ and $^3P_1 \rightarrow {}^3H_5$, $^3F_3$

Er^{3+} glass (λ_{exc} = 379 nm) : $^2H_{9/2} \rightarrow {}^4I_{15/2}$, $^4F_{5/2}$
$\rightarrow {}^4I_{15/2}$, $^4F_{7/2} \rightarrow {}^4I_{15/2}$, $^2H_{11/2} \rightarrow {}^4I_{15/2}$, $^4S_{3/2}$
$\rightarrow {}^4I_{15/2}$, $^2G_{9/2} \rightarrow {}^4I_{13/2}$, $^4F_{9/2} \rightarrow {}^4I_{15/2}$ and $^2G_{9/2} \rightarrow {}^4I_{11/2}$

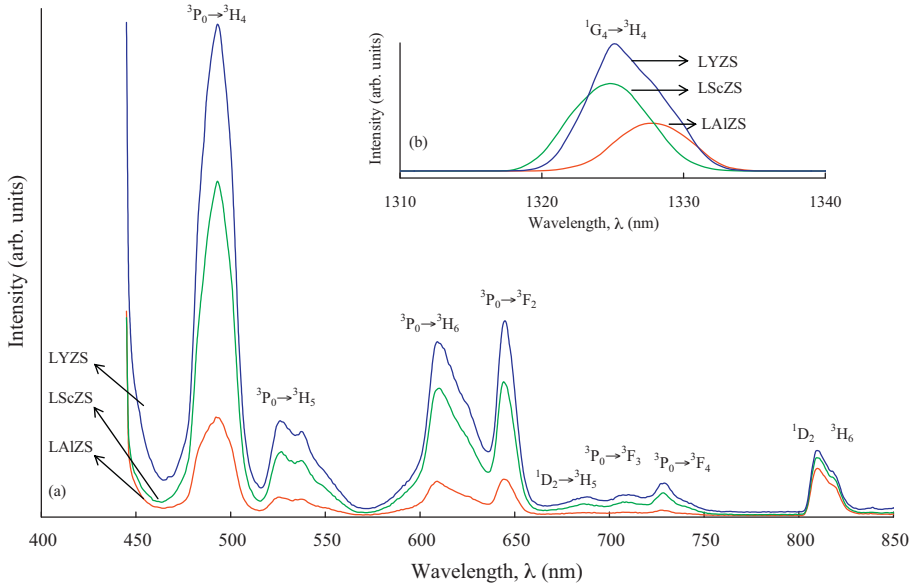

Fig. 3. Photoluminescence spectra of Pr^{3+} doped Li_2O–M_2O_3–ZrO_2–SiO_2 glasses recorded at room temperature in (a) visible and (b) NIR regions.

The spectral positions of all these bands remain virtually the same, however a considerable variation in the in the intensity of the bands could clearly be observed when the glasses are mixed with different sesquioxides.

The energy-level diagram containing the absorption and emission transitions of Pr^{3+} and Er^{3+} ions observed for one of the glasses Li_2O–Y_2O_3–ZrO_2–SiO_2 are shown in Fig. 5.Using JO intensity parameters, the radiative transition probability, radiative life time τ of an excited energy level and the branching ratio $\beta_{JJ'}$ are evaluated using the standard equations and are presented in Tables 4a and 4b.

The fluorescence decay curves of $^3P_0 \rightarrow {}^3H_4$ line of Pr^{3+} ion (Fig. 6) and also $^4S_{3/2} \rightarrow {}^4I_{15/2}$ (green emission) line of Er^{3+} ion (Fig. 7) for all the three glasses are observed to be single exponential, however at long time decay deviations from single exponential decay are clearly observed probably because of an energy transfer between ions.

4. Discussion

Among various constituents of Li_2O–Al_2O_3–ZrO_2–SiO_2 glass composition, SiO_2 is a well known glass former and expected to participate in the glass network with tetrahedral $[SiO_{4/2}]^0$ units and all the four oxygens in SiO_4 tetrahedral are shared. On addition of modifiers like Li_2O, the Si–O–Si linkage is broken and form Si–O^- termination. Thus, the structure is depolymerised and there will be a formation of meta, pyro and ortho-silicates viz., $[SiO_{4/2}]^0$, $[SiO_{3/2}O]^-$, $[SiO_{2/2}O_2]^{2-}$, $[SiO_{1/2}O_3]^{3-}$ and $[SiO_4]^{4-}$ as per the following equations:

$$2[SiO_{4/2}]^0 + Li_2O \rightarrow 2[SiO_{3/2}O]^- + 2Li^+$$

$$2[SiO_{2/2}O_2]^{2-} + Li_2O \rightarrow 2[SiO_{1/2}O_3]^{3-} + 2Li^+$$

Zirconium ions in general do participate in the glass network with ZrO_4 structural units and alternate with SiO_4 structural units.

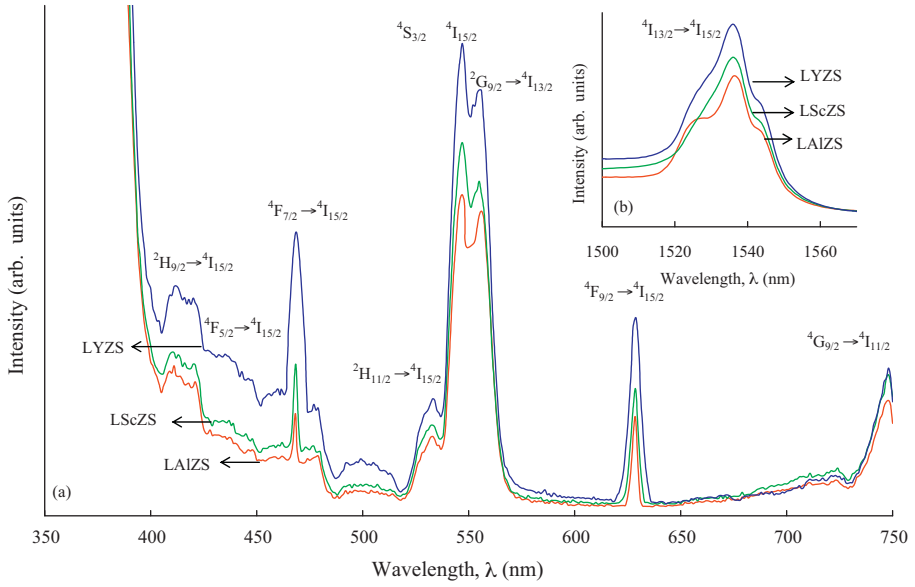

Fig. 4. Photoluminescence spectra of Er^{3+} doped Li_2O–M_2O_3–ZrO_2–SiO_2 glasses recorded at room temperature in (a) visible and (b) NIR regions.

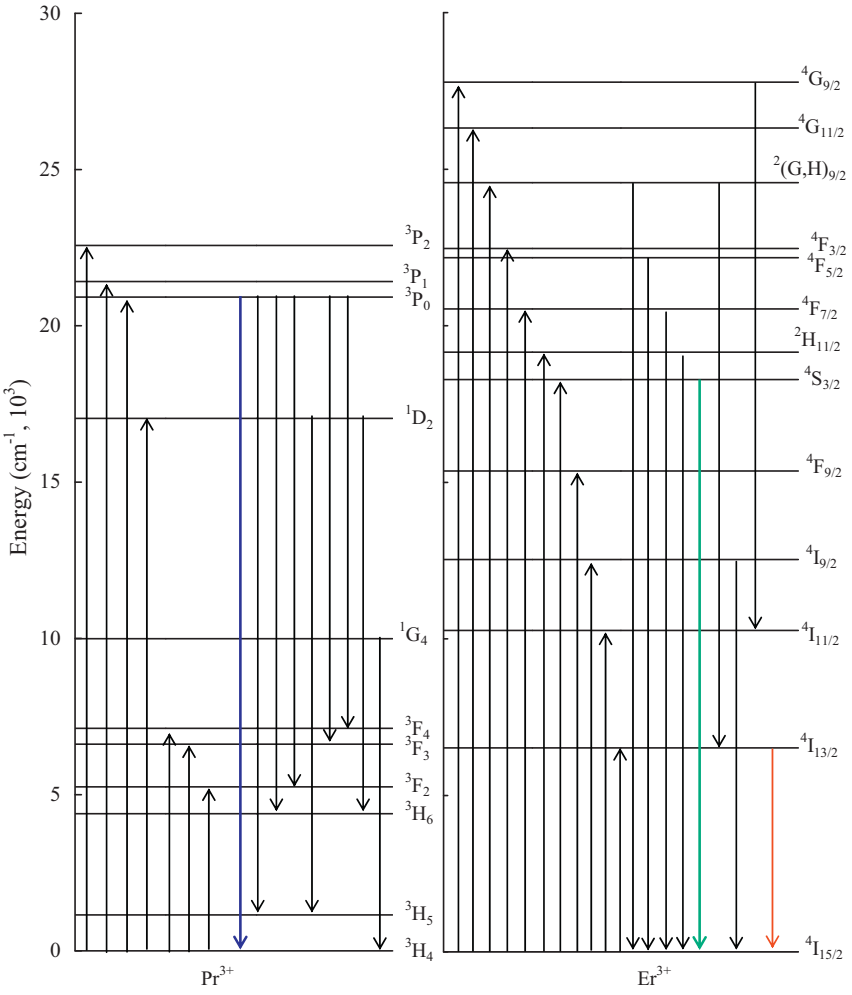

Fig. 5. The energy-level diagram containing the absorption and emission transitions of Pr^{3+} and Er^{3+} ions observed in the glass Li_2O–Y_2O_3–ZrO_2–SiO_2.

Table 4a
Various radiative properties of transitions of Pr^{3+} ions in Li_2O–M_2O_3–ZrO_2–SiO_2 glasses.

Transition	LAlZS glasses			LScZS glasses			LYZS glasses		
	Energy (cm^{-1})	A (s^{-1})	β (%)	Energy (cm^{-1})	A (s^{-1})	β (%)	Energy (cm^{-1})	A (s^{-1})	β (%)
$^3P_0 \rightarrow {}^3H_4$	20,243	18,622	48.48	20,284	19,931	53.10	20,284	19,954	54.24
$^3H_5$	19,012	2643	6.88	18,939	2556	6.81	18,975	2417	6.57
$^3H_6$	16,339	13,775	35.85	16,367	12,024	32.04	16,367	11,414	31.02
$^3F_2$	15,446	3375	8.79	15,504	3021	8.05	15,504	3001	8.16
		ΣA_{ij} = 38,415 (s^{-1})			ΣA_{ij} = 37,532 (s^{-1})			ΣA_{ij} = 36,786 (s^{-1})	
		τ = 26.0 μs			τ = 26.6 μs			τ = 27.2 μs	

This structure leads to long chains of tetrahedrons where the long chain molecules are entwined and the introduction the Ln^{3+} ions causes cross-linking of the tungsten phosphate structure. If we consider the sesquioxides (Al_2O_3, Sc_2O_3 and Y_2O_3) to be incorporated between the long chain molecules in the vicinity of Ln^{3+} ion, then the symmetry and or covalency of the glass at the Ln^{3+} ions should be different for different sesquioxides. Additionally, the variations in the concentration of different structural units of silicate groups is also expected to modify the crystal field around Ln^{3+} ions in the network. Such variations might be responsible for the observed

Table 4b
Various radiative properties of transitions of Er^{3+} ions in Li_2O–M_2O_3–ZrO_2–SiO_2 glasses.

Transition	LAlZS glasses			LScZS glasses			LYZS glasses		
	Energy (cm^{-1})	A (s^{-1})	β (%)	Energy (cm^{-1})	A (s^{-1})	β (%)	Energy (cm^{-1})	A (s^{-1})	β (%)
$^4S_{3/2} \rightarrow {}^4I_{15/2}$	18,255	7710.4	94.6	18,282	7653.1	95.17	18,315	7159.3	95.9
$\rightarrow {}^4I_{13/2}$	11,754	353	4.33	11,765	309.6	3.85	11,779	284	3.81
$\rightarrow {}^4I_{11/2}$	7885	80.3	0.98	7886	78.3	0.97	7893	20.1	0.27
		ΣA_{ij} = 8143 (s^{-1})			ΣA_{ij} = 8041 (s^{-1})			ΣA_{ij} = 7463.4 (s^{-1})	
		τ = 122 μs			τ = 124 μs			τ = 134 μs	

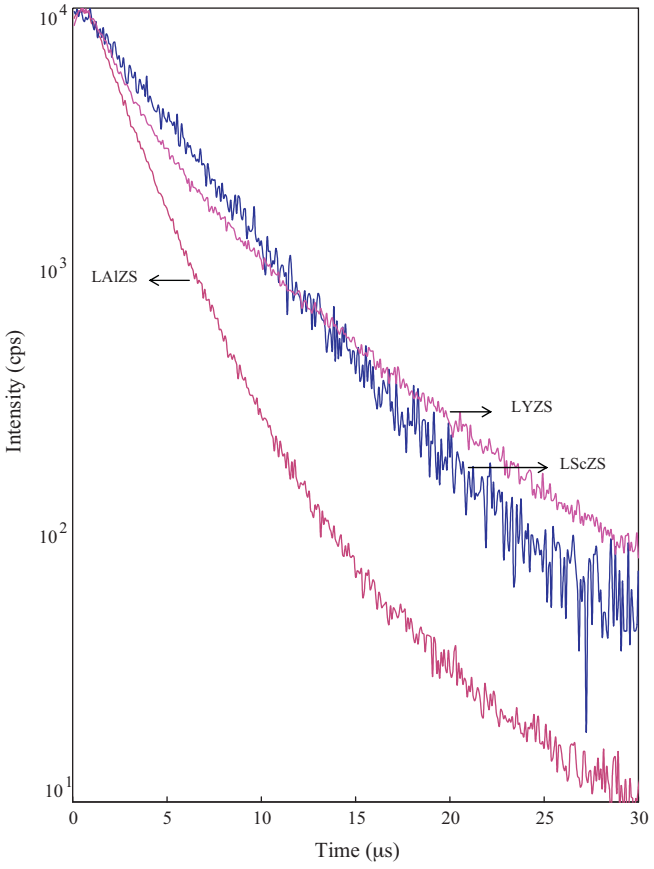

Fig. 6. Decay curves of Pr^{3+} ($^3P_0 \rightarrow {}^3H_6$) doped Li_2O–M_2O_3–ZrO_2–SiO_2 glasses recorded at room temperature.

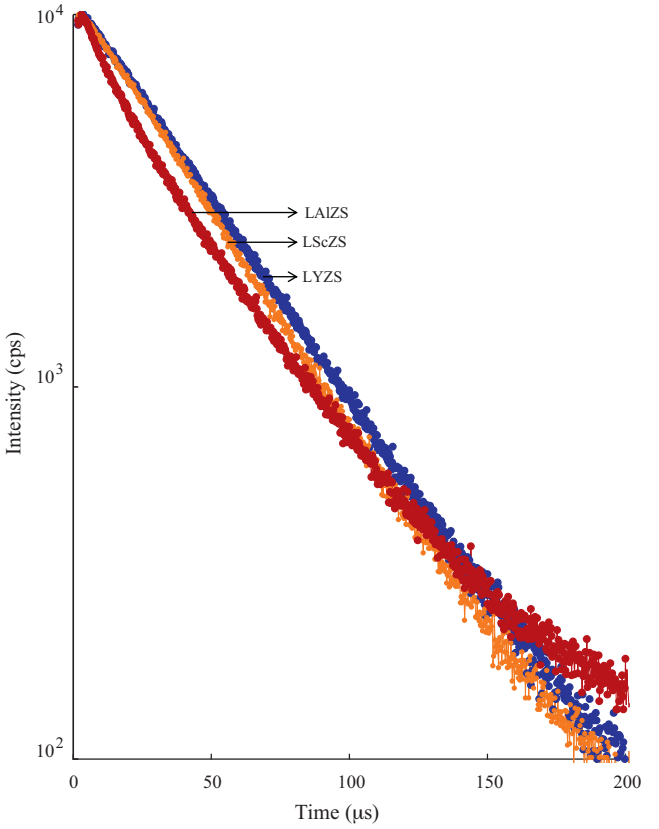

Fig. 7. Decay curves of Er^{3+} ($^4S_{3/2} \rightarrow {}^4I_{15/2}$) doped Li_2O–M_2O_3–ZrO_2–SiO_2 glasses recorded at room temperature.

differences of the luminescence intensity of various transitions of these samples.

Considering the entry of sesquioxides, yttrium ions enter in to the silicate glass network with YO_6 octahedral structural units linking either by sharing corners or edges with SiO_4 structural units [51,52].

It is necessary to emphasize that upper valence band is prevailingly originated from 2pO states. These states are relatively delocalized. This fact may play decisive role for the relaxation processes.

Al_2O_3 is an incipient glass former, as such does not form the glass by itself; however in the presence of modifiers like Li_2O it participates in the glass network. Earlier NMR studies on aluminum silicate glasses have indicated that these ions occupy mainly tetrahedral (AlO_4) and octahedral (AlO_6) sites [53]:

$$2Al_2O_3 \rightarrow [Al^{3+}]_o + 3[AlO_{4/2}]_t$$

It is common understanding that Al^{3+} is in tetrahedral coordination in aluminum silicate melts with sufficient modifying cations like Li^+ for charge-balance. Coordination transformation of Al^{3+} from a network former to a network modifier in a melt with $(Al^{3+} + Si^{4+})_2O_5^{2-}$ stoichiometry may be expressed with the formalized equation:

$$5Si_2O_5^{2-} + (LiAl)_2O_5^{2-} = 10[(SiO_3)^{2-}/(SiO_{2/2}O_2)^{2-}] + 2Li^+ + 2Al^{3+}$$

However, some previous studies on other silicate glasses containing Al_2O_3 have pointed out that Al(6) dominates the glass structure when Al_2O_3 is present in low concentrations and Al(4) structural units prevail when Al_2O_3 is present in higher concentrations [54].

The structural situation and role of the scandium species in these glasses can be thought to be similar to that for small ionic radii rare-earth cations such as Yb^{3+} or Lu^{3+}, whose ionic radii similar to Sc^{3+} which are expected to occupy octahedral positions in the glass matrices [55]. In view of this, Sc^{3+} ions are also expected to occupy octahedral positions. In fact earlier NMR studies on several Sc_2O_3 mixed oxide glasses indicated that these ions occupy octahedral positions in the glass network without direct Sc–O–Sc linkages [56–58]. However small percentage of eight-coordinate Sc atoms is also detected in some of the glasses [59].

Over all the three ions viz., Al^{3+}, Sc^{3+} and Y^{3+} are expected to be coordinated by three SiO_4 tetrahedral ligands. Two of the oxygen ions associated with each tetrahedron is assumed to be non-bridging ions forming ionic bonds with these trivalent ions (Fig. 8(a)). However in case of Y^{3+} ions silicate tetrahedra must be moved more outward since the ionic radius of this ion is more when compared with that of Al^{3+} and Sc^{3+} ions. In view of this, although three ions are linked in triangle with SiO_4 structural units, the octahedra of yttrium ion is more distorted when compared with that of the other two ions.

The energies and spectral profiles of certain transitions in the absorption spectra of Ln^{3+} ions throw some light on their coordination [60]. The energy of ~21,000 cm^{-1} for $^3H_4 \rightarrow {}^3P_0$ transition for Pr^{3+} suggest predominately 8 coordination for these ions in the present glass host [61]. These distorted PrO_8 structural units form a one-dimensional chain through edge-sharing in the glass network. Similarly there are a considerable number of studies mentioning that Er^{3+} ions do occupy 8 coordination in oxide glasses [62]. Keeping these points in mind the structural segment of the silicate glasses mixed with one of the sesquioxides (Al_2O_3) doped with Pr^{3+}/Er^{3+} ions is illustrated in Fig. 8(b).

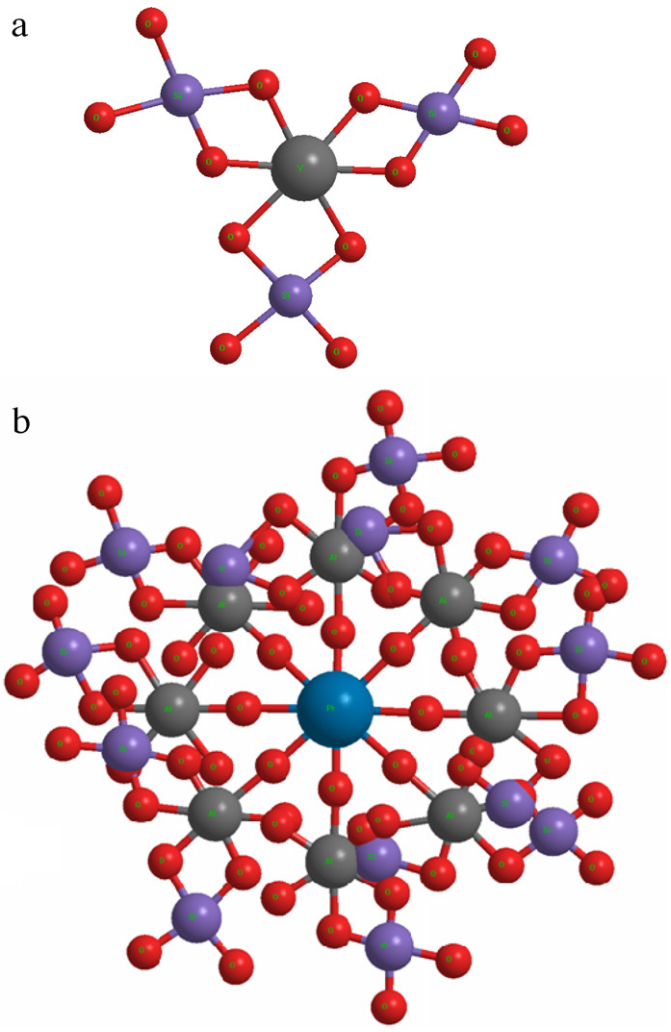

Fig. 8. Illustrations of octahedron of (a) sesquioxide surrounded by three SiO_4 units (b) Pr^{3+} ion interlocked in eight coordination in M_2O_3–SiO_2 glass network.

In general, the $^4S_{3/2} \rightarrow {}^4I_{15/2}$ green emission of Er^{3+} ions is strongly affected by multi-phonon relaxation, since the energy gap between $^4S_{3/2}$ and the lower-lying $^4F_{9/2}$ levels of erbium is about 2900 cm^{-1} and can be spanned by only three phonons; (the highest phonon energy of the host being ~1100 cm^{-1}). Such multi-phonon losses seem to be low in the glasses mixed with Y_2O_3.

The rare earth ions that occupy different coordination sites with non-centro symmetric potential contribute significantly to Ω_2 [63]. Even with similar coordination, the differences in the distortion at these ion sites may lead to a re-distribution in the crystal field. The variations in the sites with non-centro symmetric potential may arise due to the influences of the long-ranged dielectric constants of media. The covalence and structural changes in the vicinity of Pr^{3+} and Er^{3+} ions (short-range effect) leads to changes in Ω_2 value. The values of Ω_4 and Ω_6 are strongly influenced by the vibrational levels associated with the central rare earth ions bound to the ligand atoms.

The comparison of Ω_2 parameter for the two series of glasses (Table 3) shows the highest value for Al_2O_3 mixed glasses and the lowest value for Y_2O_3 mixed glasses. According to the Judd–Ofelt theory, the intensity parameters contain two terms: (i) crystal field parameter that determines the symmetry and distortion related to the structural change in the vicinity of rare earth ions. In the present context, this may be understood as follows: as it has already been mentioned that the octahedra of yttrium ion connected with the silicate groups is more distorted among octahedral of the three sesquioxides. As a result a larger average distance between Si–O–Si, Si–O–Zr chains is expected causing the average Pr–O and Er–O distance to increase. Such increase in the bond lengths produces weaker field around Pr^{3+} and Er^{3+} ions leading to lower value of Ω_2 for LYZSPr and LYZSEr glasses. (ii) The second term is the covalency between the rare earth ion and the ligand oxygen ion. For oxide glasses this is related to the radial overlapping integral of the wave functions between 4f and admixing levels, e.g. 5d, 5g and the energy denominator between these two energy terms. Thus lower value of Ω_2 for Y_2O_3 mixed glasses points out, that there is a higher degree of disorder in these glasses.

Further support for the argument that there is more structural disorder in Y_2O_3 mixed glasses than other two glasses can also be cited from the value of the bonding parameter δ; the value of δ for these glasses is found to be the lowest (more negative); this observation indicates a lower covalent environment for the rare earth ions in this glass.Branching ratio 'β' (that defines the luminescence efficiency of the transition) of the $^3P_0 \rightarrow {}^3H_4$ transition, among various transitions originated from $^3P_0$, of Pr^{3+} ions is found to be the highest for the glass mixed with Y_2O_3 (Table 4a). Similarly, the branching ratios, β values obtained for green emission level of Er^{3+} ions for the glasses mixed with the three sesquioxides are furnished in Table 4b. The comparison shows the largest value for the glass mixed with Y_2O_3 indicating that these glasses exhibit better lasing action among all other Er^{3+} doped glass series. It is also principle that Y ions possess higher polarizability with respect to other cations which effectively changes the corresponding local field splitting of the rare earth's ions localized levels.

Concerning the NIR emission, in the Er^{3+} doped glasses earlier reported that in a number of glass hosts and crystals, $^4I_{13/2}$ state of Er^{3+} ions is relatively stable and acts as a good population reservoir level [64]. This level is further populated by the transition from $^4F_{7/2}$ level (Fig. 5). Once $^4I_{13/2}$ state is populated, most of Er^{3+} ions return to $^4I_{15/2}$ ground state resulting strong ~1.54 μm emission. Further, the energy gap between $^4I_{13/2}$ and $^4I_{15/2}$ states is expected to be slightly low for Y_2O_3 mixed glasses due to the higher degree of distortion as discussed earlier. Hence losses due to multiphonon relaxation between $^4I_{13/2}$ and $^4I_{15/2}$ states can also be considered as minimal for the glass mixed with Y_2O_3. All these factors account for high NIR emission at ~1.54 μm in LYZS: Er^{3+} glass among the three Er^{3+} doped glass systems studied. A similar argument holds good for enhanced NIR emission in Y_2O_3 mixed glasses due to $^1G_4 \rightarrow {}^3H_4$ transition.

The measured fluorescence lifetimes τ are apparently shorter than calculated life times from the J–O theory (Table 5). Such difference obviously suggests some non-radiative losses.

The quantum yield (η) is defined as the radiative portion of the total relaxation rate of a given energy level [65]:

$$\eta = \frac{A_{rad}}{A_{rad} + W_{nr}} = \frac{\tau_{exp}}{\tau_{rad}} \quad (4)$$

where A_{rad} is the total radiative relaxation rate, W_{nr} is the rate of total non-radiative transition τ_{exp} – experimental lifetime, τ_{rad} – radiative lifetime. The value of η (for the $^3P_0$ level of Pr^{3+} ions and $^4S_{3/2}$ of Er^{3+} ions) determined for the three glasses is presented in Table 5. The comparison shows the highest value of η for Y_2O_3 mixed glasses. Such high value is connected not only with the higher radiative relaxation probability but also with a reduction of the non-radiative transition probability. This is possibly due to the low electron–phonon coupling of the Ln^{3+} ion with the high-energy phonons in case of Y_2O_3 mixed glasses and relatively higher degree of this coupling with low-energy phonons for Sc_2O_3 and Al_2O_3 mixed glasses.

It may be noted here that neither absorption spectroscopy nor emission spectroscopy has indicated extraordinary changes of posi-

Table 5
Data related to quantum efficiencies of the principal lines for the Li_2O–M_2O_3–ZrO_2–SiO_2: Pr^{3+}/Er^{3+} glasses.

	Pr^{3+} ($^3P_0$)			Er^{3+} ($^4S_{3/2}$)		
	LAlZS	LScZS	LYZS	LAlZS	LScZS	LYZS
Measured (τ_m) (μs)	3.9	7.3	8.9	122	124	134
Calculated (τ) (μs)	26.0	26.6	27.2	586	426	390
Quantum yield (η%)	15.0	27.4	32.7	28.6	30.8	34.3

tions of various spectral transitions due to mixing of different sesquioxides. However, the higher values of the observed experimental lifetime of $^3P_0$ state of Pr^{3+} ions and $^4S_{3/2}$ state of Er^{3+} ions in Y_2O_3 mixed glasses and also caused that the quantum yield for these samples to reach values of 32.7 and 34.3, respectively. In case of Pr^{3+} ions this decrease of non-radiative transitions concerns with the transition from $^3P_0$ to $^1D_2$. This may be understood as due to the participation of the $^1D_2$ state in the non-radiative depopulation of the $^3P_0$ level [65]. It should be emphasized that these glasses do not show any signs of nanocrystallization processes. Additional role may be played by multi-phonon relaxation processes typical for the Pr^{3+} ions [66,67].

5. Conclusions

The optical absorption and photoluminescence spectra of Pr^{3+} and Er^{3+} ions in Li_2O–ZrO_2–SiO_2: Pr_2O_3/Er_2O_3 mixed with three interesting sesquioxides (viz., Al_2O_3, Sc_2O_3, Y_2O_3) have been reported. The Judd–Ofelt theory is used to characterize the optical absorption and emission spectra of these ions. The comparison of branching ratios β_r and quantum efficiencies of $^3P_0 \rightarrow {}^3H_4$ (Pr^{3+}) and $^4S_{3/2} \rightarrow {}^4I_{15/2}$ (Er^{3+}) emissions for both the series of the glasses showed the largest values for glass mixed with Y_2O_3 among the three glasses studied. The reasons for the higher values of these parameters for Y_2O_3 mixed glasses have been discussed due to variations in the degree of disorder around rare earth ions in the glass network. The values of Ω_λ are found to be in the following order for the Pr^{3+} doped glasses: $\Omega_6 > \Omega_4 > \Omega_2$ and for Er^{3+} the order is $\Omega_2 > \Omega_4 > \Omega_6$ for all the three sets of samples. The comparison of the data on Ω_λ parameters of Pr^{3+} and Er^{3+} ions in various other glass matrices indicated the similar trends.

Acknowledgements

Two of the authors Ch. Srinivasa Rao and T. Sri Kumar wish to thank UGC, Govt. India and the Management of Andhra Loyola College, Vijayawada for sanctioning study leave under FDP.

References

[1] M. El Okra, M. Farouka, M. El-Sherbinya, M.A.K. El-Fayoumib, M.G. Brik, J. Alloys Compd. 490 (2010) 184.
[2] G. Lakshminarayana, J. Qiu, J. Alloys Compd. 476 (2009) 470.
[3] G. Lakshminarayana, H. Yang, Y. Teng, J. Qiu, J. Lumin. 129 (2009) 59–68; G. Lakshminarayana, R.V. Sagar, S. Buddhudu, J. Lumin. 128 (2008) 690–695.
[4] Y. Tian, R. Xu, L. Zhang, L. Hu, J. Zhang, Opt. Lett. 36 (2011) 109.
[5] F. Zhua, Z. Xiaoa, L. Yana, F. Zhanga, K. Zhongb, G. Cheng, Nucl. Inst. Methods 267 (2009) 3100.
[6] L. Bokatial, S. Rai, J. Lumin. 130 (2010) 1857.
[7] T. Satyanarayana, M.G. Brik, N. Venkatramaiah, I.V. Kityk, K.J. Plucinski, V. Ravikumar, N. Veeraiah, J. Am. Ceram. Soc. 93 (2010) 2004.
[8] C. Stoneman, L. Esterowitz, Opt. Lett. 15 (1990) 486.
[9] J.F. Wu, S.B. Jiang, T. Luo, J.H. Geng, N. Peyghambarian, N.P. Barnes, IEEE Photonics Tech. Lett. 18 (2006) 334.
[10] L. Feng, J. Wang, Q. Tang, L.F. Liang, H.B. Liang, Q. Su, J. Lumin. 124 (2007) 187.
[11] H. Pfeiffer, P. Bosch, S. Bulbulian, J. Nucl. Mater. 257 (1998) 309.
[12] A.R. Raffray, M.C. Billone, G. Federici, S. Tanaka, Fus. Eng. Des. 28 (1995) 240.
[13] R.R. Goncalves, J.J. Guimaraes, J.L. Ferrari, L.J.Q. Maia, S.J.L. Ribeiro, J. Non-Cryst. Solids 354 (2008) 4846.
[14] M.A. Russak, C.V. Jahnes, E.P. Katz, J. Vac. Sci. Technol. A 7 (1989) 1248.
[15] S. Banijamali, B. Eftekhari Yekta, H.R. Rezaie, V.K. Marghussian, Thermochim. Acta 488 (2009) 60.
[16] L. Fornasiero, E. Mix, V. Peters, K. Peterman, G. Huber, Cryst. Res. Technol. 34 (1999) 225.
[17] N.T. McDevitt, A.D. Davidson, J. Opt. Soc. Am. A 56 (1966) 636.
[18] J. Kong, D.Y. Tang, B. Zhao, J. Lu, K. Ueda, H. Yagi, T. Yanagitani, Appl. Phys. Lett. 86 (2005) 161116.
[19] M. Tokurakawa, K. Takaichi, A. Shirakawa, K. Ueda, H. Yagi, T. Yanagitani, A.A. Kaminskii, Appl. Phys. Lett. 90 (2007) 071101.
[20] A.O.G. Dikovska, P.A. Atanasov, M.J.D. Castro, A. Perea, J. Gonzalo, C.N. Afonso, J.G. Lopez, Thin Solid Films 500 (2006) 336.
[21] H. Guo, W. Zhang, L. Lou, A. Brioude, J. Mugnier, Thin Solid Films 458 (2004) 274.
[22] M.B. Korzenski, P. Lecoeur, B. Mercey, P. Camy, J.L. Doualan, Appl. Phys. Lett. 78 (2001) 1210.
[23] R. Krsmanovi', O.I. Lebedev, A. Speghini, M. Bettinelli, S. Polizzi, G.V. Tendeloo1, Nanotechnology 17 (2006) 2805.
[24] C.T. Horowitz, G.A. Gschneidner, Scandium , Academic, New York, 1975.
[25] V. Peters, E. Mix, L. Fornasiero, K. Petermann, G. Huber, S.A. Basun, Laser Phys. 10 (2000) 417.
[26] C. Gheorghe, A. Lupei, V. Lupei, L. Gheorghe, A. Ikesue, J. Appl. Phys. 105 (2009) 123110.
[27] Y. Cheng, H. Xiao, C. Shung, B. Tang, Physica B 404 (2009) 1230.
[28] M. Arora, S. Baccaro, G. Sharma, D. Singh, K.S. Thind, D.P. Singh, NIMS Phys. Res. B 267 (2009) 817.
[29] F.A.A. Wahab, M.A. Baki, J. Non-Cryst. Solids 355 (2009) 2239.
[30] D.U. Tulyaganov, S. Agathopoeslos, I. Kansal, P. Valerio, M.J. Ribeiro, J.M.F. Ferreira, Ceram. Int 35 (2009) 3013.
[31] H.R. Fernandes, D.U. Tulyaganov, A. Goel, M.J. Ribeiro, M.J. Pascual, J.M.F. Ferreira, J. Eur. Ceram. Soc. 30 (2010) 2017.
[32] B.R. Judd, Phys. Rev. 127 (1962) 750.
[33] G.S. Ofelt, J. Chem. Phys. 37 (1962) 511.
[34] R. Van Deun, K. Binnemans, C. Görller-Walrand, J.L. Adam, J. Alloys Compd. 283 (1999) 59.
[35] M. Malinowski, M. Kowalska, R. Piramidowicz, T. Lukasiewicz, M. Swirkowicz, A. Majchrowski, J. Alloys Compd. 323 (2001) 214.
[36] B. Klimesz, G. Dominiak-Dzik, P. Solarz, M. Zelechower, W. Ryba-Romanowski, J. Alloys Compd. 403 (2005) 76.
[37] D. Wang, S. Huang, F. You, S. Qi, H. Peng, Physica B 387 (2007) 86.
[38] E.B. Dunina, A.A. Kaminskii, A.A. Kornienko, K. Kurbanov, K.K. Pukhov, Fizika Tverdogo Tela. 32 (1990) 1568.
[39] A.A. Kornienko, A.A. Kaminskii, E.B. Dunina, Phys. Solidi Stat. B 157 (1990) 267.
[40] S. Huang, L. Lu, W.Y. Jia, X.J. Wang, W.M. Yen, A.M. Srivastava, A.A. Setlur, Chem. Phys. Lett. 348 (2001) 11.
[41] W.T. Carnall, G.L. Goodman, K. Rajnak, R.S. Rana, J. Chem. Phys. 90 (1989) 3443.
[42] C. Görller-Walrand, K. Binnemans, Handb. Phys. Chem. Rare Earths 25 (1998) 101.
[43] J. Zavadil, P. Kostka, J. Pedlikova, Z.G. Ivanova, K. Zdansky, J. Non-Cryst. Solids 356 (2010) 355.
[44] H. Inoue, K. Soga, A. Makishima, J. Non-Cryst. Solids 325 (2003) 282.
[45] Z. Mazurak, S. Bodył, R. Lisiecki, J. Gabryś-Pisarska, M. Czaja, Opt. Mater. 32 (2010) 547.
[46] L. Srinivasa Rao, M. Srinivasa Reddy, M.V. Ramana Reddy, N. Veeraiah, Physica B 403 (2008) 2542.
[47] A. Baraldi, R. Capelletti, M. Mazzera, A. Ponzoni, G. Amoretti, N. Magnani, Phys. Rev. B 72 (2005) 075132.
[48] C. Laxmikanth, B.V. Raghavaiah, B. Appa Rao, N. Veeraiah, J. Lumin. 109 (2004) 193.
[49] C.K. Jorgenson, Orbitals Atoms Molecules , Academic, London, 1962.
[50] S.P. Sinha, Complexes of the Rare Earths , Pergamon, Oxford, 1966.
[51] G. Schaack, J.A. Koningstein, J. Opt. Soc. Am. 60 (1970) 1110.
[52] D. Bloor, J.R. Dean, J. Phys. C; Solid State Phys. 5 (1972) 1237.
[53] D. Muller, G. Berger, I. Grunze, G. Ladwig, E. Hallas, U. Haubenreisser, Phys. Chem. Glasses 24 (1983) 37.
[54] Y. Gandhi, M.V. Ramachandra Rao, Ch. Srinvasa Rao, T. Srikumar, I.V. Kityk, N. Veeraiah, J. Appl. Phys. 108 (2010) 023102.
[55] N. Purnachand, T. Satyanarayana, I.V. Kityk, N. Veeraiah, J. Alloys Compd. 492 (2010) 706.
[56] H. Park, I. Bull, L. Peng, V.G. Young Jr., C.P. Grey, J.B. Parise, Chem. Mater. 16 (2004) 5350.
[57] D. Riou, F. Fayon, D. Massiot, Chem. Mater. 14 (2002) 2416.
[58] S.R. Miller, A.M.Z. Slawin, P. Wormald, P.A. Wright, J. Solid State Chem. 178 (2005) 1738.

[59] D. Mohr, A.S.S. de Camargo, C.C. de Araujo, H. Eckert, J. Mater. Chem. 17 (2007) 3733.
[60] Q. Su, Y. Lu, Rare Earth Spectroscopy , World Science, New York, 1985.
[61] V. Ravikumar, N. Veeraiah, B. Appa Rao, J. Lumin. 75 (1997) 57.
[62] P. Nachimuthu, R. Jagannathan, Phys. Chem. Glasses 36 (1995) 204.
[63] Y. Sakurai, K. Nagasawa, H. Nishikawa, Y. Ohki, J. Appl. Phys. 86 (1999) 370.
[64] I.V. Kityk, J. Wasylak, D. Dorosz, J. Kucharski, A. Brenier, Mater. Lett. 51 (2001) 194.
[65] M. Rozanski, K. Wisniewski, J. Szatkowski, Cz. Koepke, M. Sroda, Opt. Mater. 31 (2009) 548.
[66] A. Brenier, I.V. Kityk, J. Appl. Phys. 90 (2001) 232.
[67] A. Majchrowski, I.V. Kityk, E. Mandowska, A. Mandowski, J. Ebothe, T. Lukasiewicz, J. Appl. Phys. 100 (2006) 053101.